Article submitted to: High Power Laser Science and Engineering, 2025 *September 11, 2025*

Generation of Intense Ultrashort Deep-Ultraviolet Pulses at 200 nm

Xinhua Xie[1], Sharon Soultanis[1], Gregor Knopp[1], Adrian L. Cavalieri[1,2], and Steven L. Johnson[1,3]

[1]*Center for Photon Science, Paul Scherrer Institute, Forschungsstrasse 111, 5232 Villigen PSI, Switzerland*
[2]*Institute of Applied Physics, University of Bern, 3012 Bern, Switzerland*
[3]*Institute for Quantum Electronics, Physics Department, ETH Zurich, CH-8093 Zurich, Switzerland*

Abstract
We report the generation of intense deep ultraviolet pulses at 200 nm with a duration of 48 fs and pulse energy of 130 μJ, achieved via cascaded sum frequency generation using 800 nm femtosecond pulses in barium borate crystals. Efficient frequency up-conversion is realized by optimizing phase-matching conditions and implementing dispersion control, while maintaining the ultrashort pulse characteristics. The generated deep ultraviolet pulses are characterized using two-photon absorption frequency-resolved optical gating, providing detailed insight into their temporal profile and phase. This approach addresses key challenges in ultrashort deep ultraviolet pulse generation, delivering a high-energy, ultrashort source suitable for ultrafast spectroscopy, nonlinear optics, and strong-field physics. These results represent a significant advancement in the generation of high-energy, ultrashort deep ultraviolet pulses, opening new possibilities for time-resolved investigations in ultrafast molecular dynamics, as well as emerging applications in semiconductor science, quantum materials, and photochemistry.

1. Introduction

The generation of intense and ultrashort deep-ultraviolet (DUV) pulses is essential to advance time-resolved spectroscopy and nonlinear optical studies in the DUV spectral range[1–4]. In particular, sub-100 femtosecond pulses at wavelengths around 200 nm enable the investigation of ultrafast electronic and nuclear dynamics in biomolecules, semiconductors, and novel materials, where strong electronic transitions and resonant nonlinear interactions occur[5–7]. The pulse duration is critical in resolving nuclear motion in photon-induced molecular processes, as vibrational wavepackets evolve on femtosecond timescales[8–14]. Shorter pulses provide higher temporal resolution, allowing the direct observation of coherent nuclear wave packet dynamics, conical intersections, and ultrafast photodissociation pathways[15]. For example, in biomolecular systems such as DNA bases, femtosecond DUV pulses enable the tracking of ultrafast nonradiative relaxation through conical intersections[16]. Similarly, in semiconductor nanomaterials, high-energy DUV pulses can be used to probe carrier relaxation dynamics and excitonic effects on ultrafast timescales[17,18]. Additionally, in strong-field physics, intense sub-100 fs pulses in the DUV regime open new avenues for investigating high-harmonic generation[19] and nonlinear optical processes in highly correlated materials[20].

Beyond fundamental spectroscopy, ultrashort DUV pulses have critical applications in seeding high-gain, high-harmonic free-electron lasers (FELs)[21–23]. The high coherence and short pulse duration of a DUV seed pulse can significantly improve the performance of FELs by reducing temporal jitter and enhancing pulse stability in extreme ultraviolet and soft X-ray regimes[24,25]. Seeding FELs with DUV pulses allows for the generation of coherent, high-brightness FEL pulses with improved spectral purity, which is essential for applications in ultrafast atomic, molecular, and condensed matter physics[26]. The ability to generate intense 200 nm pulses with precise temporal control is therefore a key step in advancing FEL technology and its applications in ultrafast science.

Various approaches have been explored for the generation of femtosecond pulses around 200 nm, each with different trade-offs in terms of energy, duration, and tunability. Frequency up-conversion through harmonic generation and four-wave mixing of femtosecond laser pulses remains a widely used technique, producing pulses in the range from a few to hundreds of femtoseconds[27–32]. Harmonic generation in gases enables the production of sub-10 fs pulses with extreme

Correspondence to: xinhua.xie@psi.ch

10.1017/hpl.2025.10084
https://doi.org/10.1017/hpl.2025.10084 Published online by Cambridge University Press

spectral broadening in the DUV spectral region, making it highly valuable for time-resolved studies[33–35]. However, this approach typically yields relatively low pulse energies, limiting its applicability in energy-demanding experiments. Dispersive wave emission in gas-filled hollow-core fibers has demonstrated few-femtosecond DUV pulses at microjoule levels with high repetition rates[36]. Metasurface-based approaches offer a novel pathway for DUV pulse generation, although they remain in early stages of development[37].

Despite significant progress, achieving high-energy (above 100 μJ) pulses with durations below 50 fs at around 200 nm remains a technical challenge due to phase-matching constraints, dispersion management, and nonlinear absorption[38]. In this work, we demonstrate the generation of intense 200 nm pulses with 48 fs duration and 130 μJ pulse energy by frequency upconversion of 800 nm femtosecond pulses using cascaded sum frequency generation in β-barium borate (BBO) crystals. The pulse energy and pulse duration of the generated 200 nm beam is optimized through phase-matching and dispersion control.

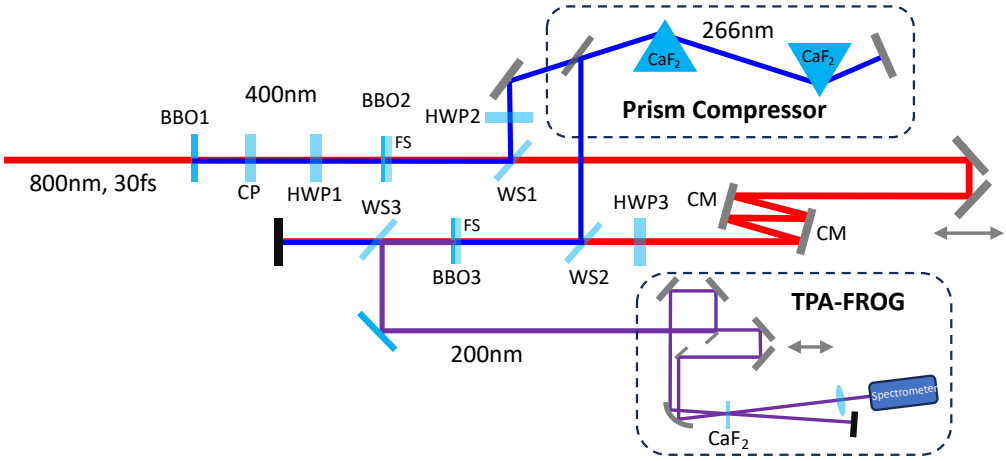

Figure 1. Schematic of the experimental setup for fourth-harmonic generation at 200 nm. BBO1: 200 μm Type I SHG BBO of 800 nm. BBO2: 50 μm Type I SFG of 800 nm and 400 nm. BBO3: 50 μm Type I SFG of 800 nm and 267 nm. CP: Time delay compensation plate. HWP1: Half-wave plate for 800 nm (also acts as a full-wave plate for 400 nm). HWP2: Half-wave plate for 267 nm. HWP3: Half-wave plate for 800 nm. WS1, WS2: Wave separators with high reflectivity for 267 nm and high transmission for 400 nm/800 nm. WS3: Wave separator with high reflectivity for 200 nm. CM: chirped mirrors for 800nm. FS:fused silica substrate.

2. Experiment

The experimental setup for the generation and characterization of DUV pulses at around 200 nm through a three-stage nonlinear frequency conversion process is illustrated in Fig. 1 using a collimated input beam from a Ti:sapphire laser amplifier (Coherent Legend Elite Duo HE+) delivers 20 mJ, 30 fs pulses at a central wavelength of 800 nm with a repetition rate of 100 Hz.

In the first stage, second-harmonic generation (SHG) occurs in the first β-BBO crystal (BBO1, 200 µm thickness), where a portion of the 800 nm fundamental beam is converted into its second harmonic at 400 nm. To compensate for the group velocity mismatch between the generated 400 nm and residual 800 nm beams, a α-BBO compensation plate (CP) is placed immediately after BBO1. A half-wave plate (HWP1) then rotates the polarization direction of the 800 nm beam by 90 degrees to ensure Type-I phase matching in the subsequent sum-frequency generation (SFG) stage.

In the second stage, sum-frequency generation takes place in the second β-BBO crystal (BBO2, 50 µm thickness with a 2-mm fused silica substrate), where the 800 nm and 400 nm pulses mix to generate 267 nm radiation. A wave separator (WS1) directs the generated 267 nm beam while transmitting the residual 400 nm and 800 nm components. Before further nonlinear conversion, the 267 nm beam is sent into a prism compressor, where its group velocity dispersion can be precisely controlled. To minimize reflection losses from the prism surfaces with Brewster incident angle, a half-wave plate (HWP2) is used to change the polarization of the 267 nm beam to the vertical direction. Additionally, the polarization of the 800 nm beam is rotated by another 90 degrees using a half-wave plate (HWP3), ensuring Type-I phase matching for the final SFG process. A pair of chirped mirrors with four bounces are used for the 800 nm beam to compensate for the group delay dispersion introduced by the optics in the beam path. The 400 nm beam is removed through the 800 nm highly reflective mirrors along

https://doi.org/10.1017/hpl.2025.10084 Published online by Cambridge University Press

the beam path.

In the third and final stage, the 267 nm and 800 nm pulses are combined in a third β-BBO crystal (BBO3, 50 µm thickness with a 2-mm fused silica substrate) via sum-frequency generation, producing the desired 200 nm DUV pulses. At 100 μJ pulse energy level, the 200 nm beam experiences more than 20% loss through a 2 mm fused silica substrate due to two-photon absorption, and significant pulse broadening from its high group-velocity dispersion (>360 fs^2/mm). To avoid these effects, the fused silica side is placed upstream, preventing the generated 200 nm pulses from passing through it. The time delay between the fundamental and the third harmonic beams is adjusted with a delay stage. A sequence of dielectric wave separators (WS1, WS2, and WS3) selectively transmits or reflects different wavelength components: WS1 and WS2 transmit 400 nm and 800 nm while reflecting 267 nm, whereas WS3 is highly reflective for the generated 200 nm pulses. Three additional WS3 elements (not shown) further suppress any remaining undesired harmonic components, ensuring a clean 200 nm output.

Efficient SHG and SFG require precise phase matching. In the present work, Type I ($o + o \rightarrow e$) phase matching is employed for all three nonlinear conversion stages. The corresponding cutting angles of the β-BBO crystals, determined from the Sellmeier equations[39], are 29.2° for SHG of 800 nm, 44.3° for SFG of 800 nm and 400 nm, and 64.9° for SFG of 800 nm and 267 nm. These angles were selected to satisfy the collinear phase-matching condition at room temperature, ensuring optimal overlap of the interacting waves.

The crystal thickness is also a critical design parameter, as it directly determines the spectral acceptance bandwidth for phase matching. Thinner crystals provide broader acceptance, which is advantageous for ultrashort pulses with large spectral bandwidths. In our configuration, the full width at half maximum (FWHM) spectral bandwidth of the fundamental 800 nm beam is approximately 48 nm. The generated 400 nm radiation exhibits a FWHM spectral bandwidth of about 8.9 nm, while the 267 nm output has a bandwidth of approximately 3.6 nm. For the 200 nm generation stage, the calculated spectral acceptance bandwidths are approximately 18 nm (FWHM) for the 800 nm input and about 4 nm for the 267 nm input. The spatial walk-off of the extraordinary wave (200 nm) at the phase matching angle is approximately 5μm over a crystal thickness of 50μm, which is negligible. The group-velocity mismatch between the 800 nm and 267 nm ordinary-polarized pulses is approximately 45 fs over a 50 μm interaction length in the crystal. These values are consistent with the expected scaling of acceptance bandwidth with crystal thickness and wavelength, and they highlight the trade-off between conversion efficiency and bandwidth preservation in multi-stage nonlinear frequency conversion.

To characterize the temporal and spectral properties of the generated DUV pulses, a two-photon absorption frequency-resolved optical gating (TPA-FROG) setup is employed. The TPA-FROG technique has been previously demonstrated for visible and infrared pulses[40–43]. FROG is a powerful technique for ultrashort pulse characterization, allowing for accessing both the intensity and phase of a pulse by generating a spectrally resolved nonlinear signal as a function of time delay[44,45]. In contrast to traditional autocorrelation techniques, which provide only partial temporal information, FROG enables full phase retrieval, making it a highly accurate and widely adopted method for ultrafast optics[46]. In our experiment, the 200 nm pulses are focused into a calcium fluoride (CaF_2) crystal with a thickness of 100 μm, where nonlinear two-photon absorption occurs, generating a signal that varies as a function of the delay between two copies of the pulse. The spectrally resolved signal is then recorded by a spectrometer. Using the FROG retrieval algorithm, the full temporal profile and spectral phase of the pulse can be reconstructed, providing precise measurements of pulse duration[46].

3. Results and Discussion

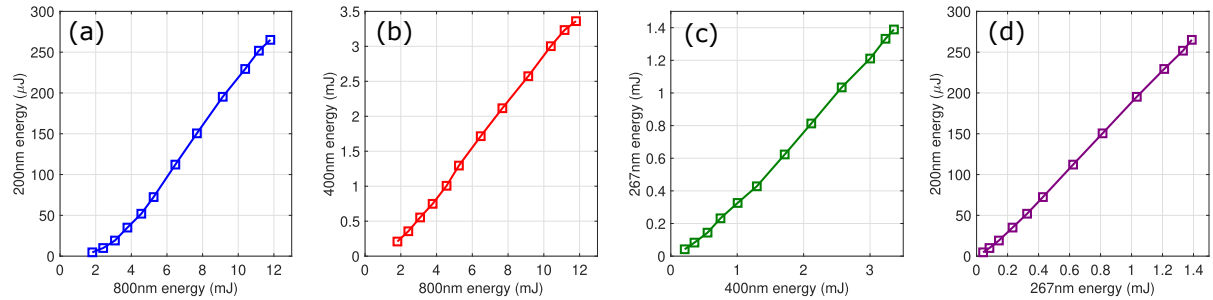

Figure 2. Measured pulse energies across the harmonic conversion stages leading to 200 nm generation. (a) Pulse energy of the 200 nm output as a function of the input 800 nm energy. (b) Conversion from 800 nm to the intermediate 400 nm second harmonic. (c) Pulse energy scaling between 400 nm and the generated 267 nm third harmonic. (d) Final frequency conversion from 267 nm to 200 nm.

In the experiment, the maximum input pulse energy is set to 18 mJ with a beam diameter of 13 mm. Due to the limited aperture size of the BBO crystals (10 mm in diameter), only 11.8 mJ of pulse energy effectively passes through the nonlinear

https://doi.org/10.1017/hpl.2025.10084 Published online by Cambridge University Press

crystals. The peak intensity at the first BBO is about 8.5×10^{11}W/cm^2. As a result, the generated fourth-harmonic pulse at 200 nm achieves a maximal energy of 265 μJ, corresponding to an overall conversion efficiency of 2.2%.

In the first SHG stage (800 nm → 400 nm), the output pulse energy at 400 nm is 3.36 mJ from an 800 nm input of 11.8 mJ, corresponding to a conversion efficiency of approximately 28.5%. In the second stage (SFG of 800 nm and 400 nm → 267 nm), the 267 nm output pulse energy is 1.39 mJ. Owing to pump depletion in the preceding stages, the residual 800 nm pulse energies are 7.8 mJ at the input to the second stage and 6.6 mJ at the input to the third stage.

To characterize the efficiency and energy scaling behavior of the cascaded harmonic generation process, we measured the output pulse energies at each stage of frequency conversion, beginning with the fundamental 800 nm beam and culminating in the final 200 nm output. The results are summarized in Fig. 2, which presents the measured energies across all nonlinear conversion stages. The pulse energy of the 800 nm beam was adjusted by rotating a half-wave plate placed before the 800 nm grating compressor, which effectively acts as a polarizer.

In Fig. 2(a), the 200 nm output energy is plotted as a function of the input 800 nm energy. A nonlinear relationship is observed at low input energies, with the 200 nm energy increasing rapidly at higher fundamental intensities. This behavior is consistent with the high-order nonlinear nature of the FHG process. As the 800 nm pulse energy reaches approximately 5 mJ, the relationship transitions to a linear regime. Saturation effects begin to appear modestly beyond 11 mJ. Figure 2(b) shows the measured second harmonic (400 nm) energy as a function of the 800 nm input. The energy scaling is nearly quadratic at lower input levels and becomes more linear at higher energies, suggesting the onset of nonlinear absorption and/or pump depletion effects. The subsequent THG from 400 nm to 267 nm is presented in Fig. 2(c). In this stage, the 267 nm output scales nearly linearly with the 400 nm input energy, demonstrating stable and efficient THG performance. The maximum output energy reaches approximately 1.39 mJ, with a consistent slope across the entire measured range, indicating favorable phase-matching and low absorption at this wavelength. Finally, Fig. 2(d) illustrates the energy scaling of the 200 nm output as a function of the 267 nm input energy. A quasi-linear trend is again observed, indicating that the final harmonic conversion step preserves high efficiency with minimal saturation effects. These results validate the sequential harmonic generation scheme and confirm that each stage contributes constructively to the overall system efficiency. Overall, the cascaded harmonic conversion system demonstrates efficient energy transfer across all stages, with no significant energy bottlenecks. The observed energy scaling behaviors highlight both the high quality of the nonlinear crystals employed and the effectiveness of the temporal synchronization and phase-matching strategies used in the setup.

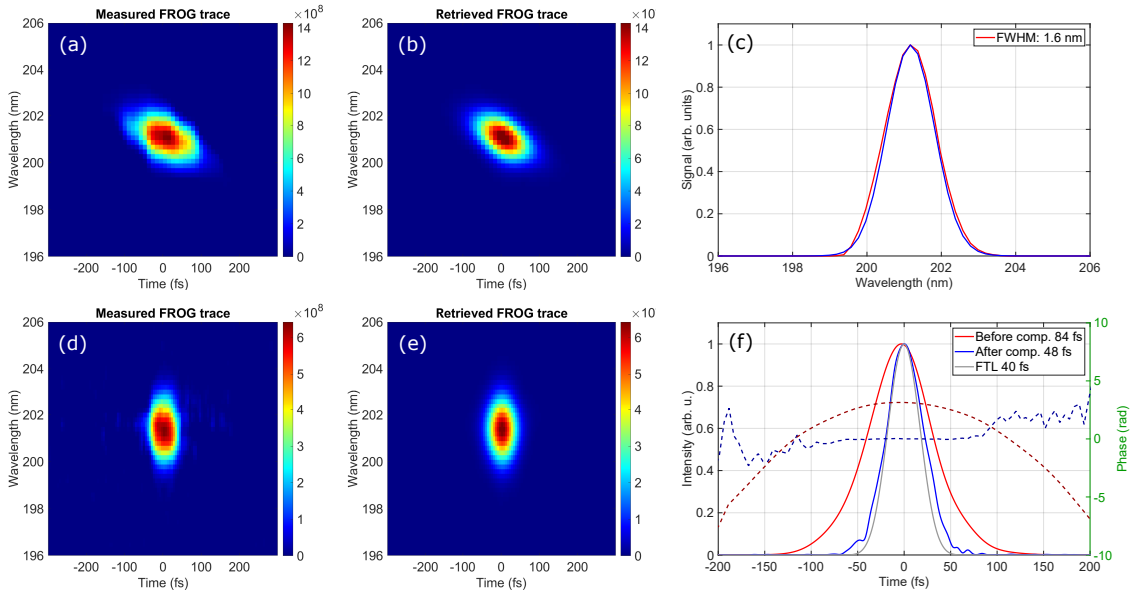

Figure 3. The measured and reconstructed TPA-FROG traces with the optimization of pulse energy (a,b) and the optimization of pulse duration (d,e) through the dispersion control of the 267 nm beam using the prism pair compressor. (c) Measured and retrieved spectra of the 200 nm beam for the measurement of (a). (f) The reconstructed temporal intensity and phase of the uncompressed and compressed pulses from (a) and (d), together with the temporal profile of the Fourier-transform limited pulse.

The measured spectrum of the 200 nm pulse, shown in Fig. 3(c), is centered at 201 nm with a FWHM bandwidth of about 1.6 nm, supporting a Fourier-transform limited (FTL) pulse duration of 40 fs. To fully characterize the temporal properties of the pulse, we perform TPA-FROG measurements. The measured and retrieved FROG traces are shown in Fig. 3(a) and (b),

https://doi.org/10.1017/hpl.2025.10084 Published online by Cambridge University Press

respectively. The FROG trace exhibits a noticeable tilt, indicating the presence of significant second-order dispersion in the pulse. The reconstructed temporal profile and the corresponding spectral phase are presented in Fig. 3(d), yielding a pulse duration of 84 fs. The retrieved parabolic spectral phase indicates a group delay dispersion (GDD) of approximately 1050 fs^2. This dispersion originates from the sum frequency generation process in the case of optimizing the 200 nm pulse energy. The presence of residual second-order dispersion highlights the need for further dispersion compensation to achieve even shorter pulse durations, potentially pushing the pulses closer to their transform limit of 40 fs.

Pulse compression of the generated 200 nm pulses is investigated using two distinct approaches to optimize the pulse duration while balancing energy loss due to material absorption and nonlinear effects. The first method employs a CaF_2 prism pair to directly compress the 200 nm pulses after generation. Using this setup, we achieve a compressed pulse duration of 49 fs. However, due to the strong two-photon absorption in CaF_2 at 200 nm, approximately 92% of the pulse energy is lost, significantly reducing the overall pulse energy to around 22 μJ.

Given the strong dispersion and absorption exhibited by most optical materials at 200 nm, an alternative approach is explored to achieve self-compression of the 200 nm pulses by controlling the dispersion of the incoming beams, which has been broadly used in second harmonic and sum frequency generation[47–52]. The first strategy involves adjusting the dispersion of the fundamental 800 nm beam using the grating compressor located before the DUV generation setup. This adjustment directly affects the generation of both the 400 nm and 267 nm pulses in the nonlinear crystals. By introducing an additional dispersion of -4760 fs^2 to the fundamental beam, we achieved compressed 200 nm pulses with a duration of 46 fs. However, this method results in a pulse energy drop to 28 μJ, mainly due to reduced conversion efficiencies for the generation of the 400 nm and 267 nm with the strongly pre-chirped 800 nm beam.

While keeping the conditions for the first two stages unchanged, a more effective approach involves dispersion control of the 267 nm beam alone, adding the CaF_2 prism compressor prior to the last stage through adjusting the position of the second prism along the beam path, as shown in Fig. 1. This method enables the direct generation of compressed 200 nm pulses from the BBO crystal, resulting in a pulse duration of 48 fs while maintaining a pulse energy of 130 μJ. The overall conversion efficiency from the driving 800 nm to DUV is 1.1%. The pre-chirp added to the 267nm is about -1520 fs^2 according to the position changes of the second prism in the compressor. The measured FROG trace, along with the retrieved trace and reconstructed pulse, are presented in Fig. 3 (d, e, f). The vertical shape of the FROG trace indicates minimal residual GDD in the pulse, leading to a flat spectral phase as shown in Fig. 3(e). This flat phase profile confirms effective dispersion management, resulting in near-optimal pulse compression with the pulse duration close to the Fourier-transform-limit.

Importantly, this technique minimizes energy losses while providing better control over the pulse duration, demonstrating a more efficient pathway for generating high-energy, ultrashort DUV pulses. These results highlight the critical role of dispersion management in optimizing pulse compression at 200 nm. The combination of CaF_2 prism compression and proper phase-matching conditions achieves a balance between pulse duration and energy, paving the way for enhanced performance in time-resolved spectroscopy, nonlinear optics, and ultrafast molecular dynamics studies in the DUV spectral range.

4. Beam spatial quality and stability

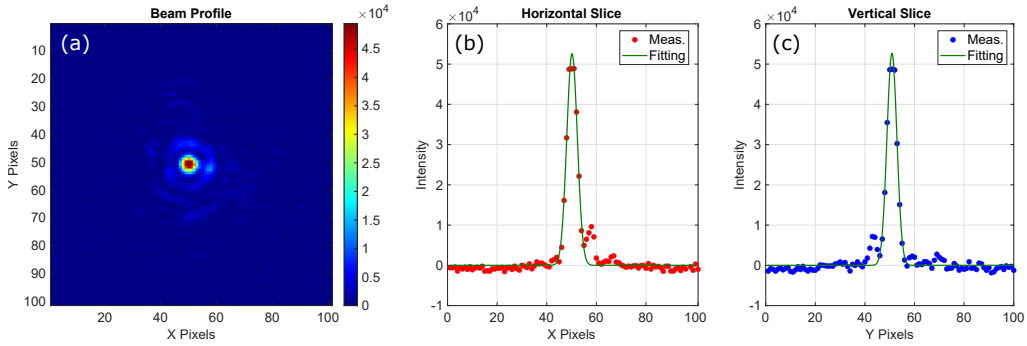

Figure 4. (a) Beam profile of the 200 nm at the focal plane of a CaF_2 lens (focal length: 500 mm) recorded with a CMOS camera. (b) and (c) show cross-sectional intensity profiles at the focal center along the horizontal and vertical directions, respectively. The CMOS camera has a pixel size of 5.5 μm.

Spatial beam quality is a critical parameter for precision applications such as FEL injection. To evaluate the spatial characteristics of the 200 nm beam, we performed a beam profile measurement at the focal plane of a CaF_2 lens with a focal length of 500 mm, using a UV-sensitive CMOS camera (pixel size: 5.5 μm). The resulting image, shown in Fig. 4, reveals a well-defined, round, and symmetric focus. Cross-sectional intensity profiles along the horizontal and vertical axes

https://doi.org/10.1017/hpl.2025.10084 Published online by Cambridge University Press

are presented in Fig. 4(b) and (c), respectively, with Gaussian fits yielding FWHM values of 27.6 μm and 26.0 μm. It is worth noting that the minor ring structures observed around the focal spot originate from the limited aperture of the BBO crystal (10 mm diameter) relative to the fundamental beam size ($1/e^2$ diameter of 13 mm). These profiles exhibit minimal asymmetry and low background noise, indicating high spatial fidelity. This measurement reinforces the conclusion that the 200 nm output maintains excellent spatial quality, making it well-suited for demanding applications such as FEL injection and precision spectroscopy.

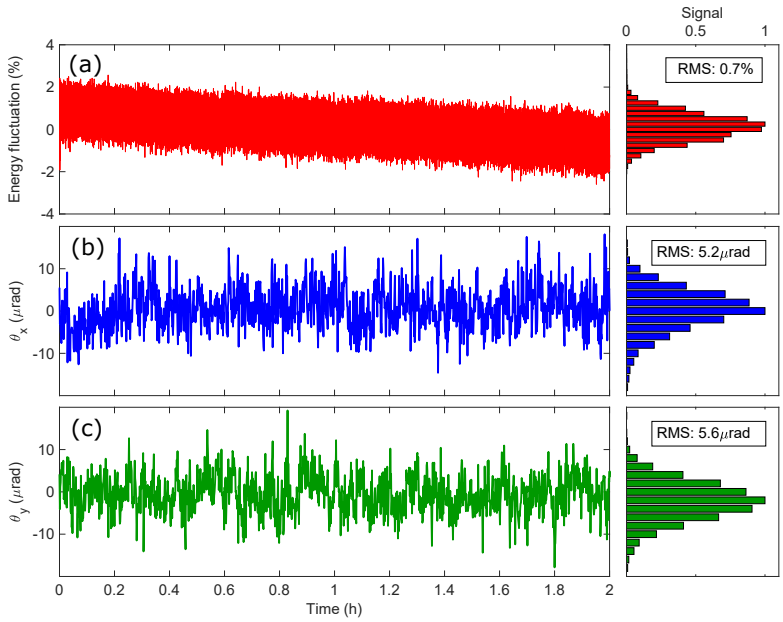

Figure 5. Single-shot measurements of pulse energy stability (a), and beam pointing along the horizontal (θ_x) and vertical (θ_y) directions (b), (c) over 2 hours for the compressed 200 nm beam. The histograms of the normalized stability distributions are plotted on the corresponding right-hand side panels.

The stability of laser fluence at the interaction point is a critical parameter for ensuring the reproducibility and accuracy of time-resolved measurements. This stability is predominantly governed by the consistency of pulse energy and beam pointing. To maintain optimal experimental conditions over extended operation periods, it is imperative to suppress fluctuations in both parameters. To assess energy and beam-pointing stability, single-shot measurements of the pulse energy and beam pointing of the compressed fourth harmonic beam were recorded continuously over 2 hours. The Ti:Sapphire laser amplifier exhibited an rms energy stability of 0.15% over 24 hours for the fundamental beam. The measured pulse energy of the fourth harmonic beam over a 2-hour period, shown in Fig. 5(a), demonstrates an rms stability of 0.7%, which is well within acceptable limits for most time-resolved applications. The beam-pointing stability was evaluated by imaging the collimated beam onto a CCD camera positioned at the focus of an uncoated CaF_2 lens with a focal length of 100 mm. The beam positions along the horizontal and vertical directions were determined by fitting the recorded beam profile to a 2D Gaussian function. Angular pointing deviations were then calculated by dividing the variations in peak position by the focal length of the lens. The resulting angular pointing stabilities of the compressed DUV pulses were 5.2 μrad (rms) horizontally and 5.6 μrad (rms) vertically, as shown in Fig. 5(b, c). These results confirm that the DUV beam exhibits excellent stability in both energy and beam pointing, making it well-suited for demanding ultrafast spectroscopy and nonlinear optical applications.

5. Comparison

Figure 6 presents a comparative analysis of pulse duration and pulse energy for DUV pulses near 200 nm, achieved in this work using cascaded SFG, alongside previous results from all-solid-state platforms [29–32]. The referenced studies encompass several notable approaches: KBBF-crystal-based generation [30], dual broadband frequency doubling (BFD) [29], cascaded SFG using BBO crystals [31], and a common-path fourth-harmonic generation (FHG) technique [32].

Among these, Zhou et al. demonstrated a pulse duration of 45 fs and a conversion efficiency of 1.5% at a central wavelength of 220 nm using the dual BFD method [29]. However, extending this technique to shorter wavelengths such as 200 nm presents challenges due to the significantly narrower phase-matching bandwidth. This limitation arises because 200 nm lies close to the bandgap of BBO at 193 nm [53], rendering efficient frequency conversion difficult and potentially precluding the use of the

https://doi.org/10.1017/hpl.2025.10084 Published online by Cambridge University Press

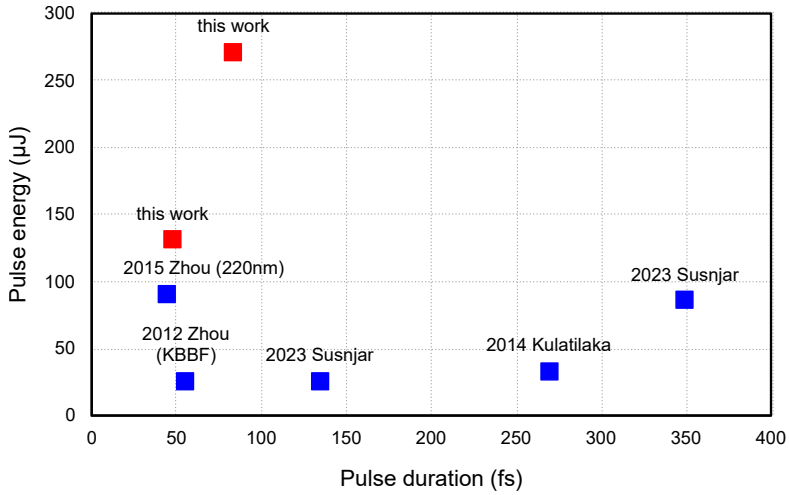

Figure 6. A summary of pulse durations and energies for experimentally demonstrated intense 200 nm pulses with all-solid setups.

dual BFD scheme in this spectral region.

In contrast, our approach advances the energy performance of DUV pulse generation by delivering pulse energies exceeding 200 μJ while preserving sub-100 fs durations. Through meticulous dispersion management of the intermediate 267 nm beam, we further compress the pulses to durations below 50 fs maintaining a pulse energy exceeding 100 μJ. This enhancement in temporal resolution is critical for high-precision ultrafast spectroscopy and nonlinear optical experiments, particularly those requiring both high photon flux and sub-50 fs time resolution in the DUV regime.

These results underscore the efficiency, stability, and scalability of our method for generating intense, ultrashort DUV pulses, representing a significant improvement over previously reported techniques in terms of both energy and duration performance.

6. Conclusion and outlook

We have demonstrated a compact, all-solid-state platform for the generation of intense, sub-50fs DUV pulses at 200 nm with pulse energies up to 130 μJ, achieved via cascaded sum-frequency generation in BBO crystals pumped by 800 nm femtosecond pulses. By optimizing phase-matching conditions, implementing precise dispersion control, and minimizing nonlinear absorption, the system achieves high conversion efficiency while preserving pulse duration and beam quality. The resulting DUV pulses are well-suited for pump–probe spectroscopy, strong-field physics, and nonlinear optical studies in the DUV regime.

Comprehensive temporal and spectral characterization using TPA-FROG proved critical, particularly given the lack of conventional nonlinear characterization techniques in the DUV range. TPA-FROG provided accurate pulse duration measurements and exposed residual phase distortions, guiding iterative refinement of the dispersion compensation scheme.

The demonstrated scheme for generating 200 nm pulses is general and can be adapted to other DUV and even shorter wavelengths. By selecting nonlinear crystals with suitable transparency and phase-matching properties, the cascaded sum-frequency generation concept can be extended into the vacuum-ultraviolet(VUV). For example, KBBF crystals support phase matching down to approximately 160 nm[54]. This versatility makes the approach broadly applicable to a wide range of ultrafast DUV and VUV light sources.

This work addresses key limitations of existing DUV generation schemes by providing a well-balanced approach that combines high pulse energy, ultrashort duration, and system simplicity. Compared to high-order harmonic generation, dispersive wave emission in photonic crystal fibers, and gas-based filamentation, our cascaded-SFG technique offers improved energy conversion and effective pulse compression, while maintaining straightforward alignment and operational robustness. Its inherent scalability and stability present promising opportunities for time-resolved studies in molecular spectroscopy, nonlinear optics, and strong-field physics across the DUV spectral range.

Future efforts will aim to advance pulse compression strategies, broaden wavelength tunability, and embed this source into experimental platforms for next-generation ultrafast spectroscopy[55–57]. Moreover, prospects for scaling pulse energy and repetition rates will be explored to meet the growing demands of high-throughput experimental workflows. Together, these developments represent a significant step toward the realization of high-energy, sub-50 fs DUV sources at around 200 nm,

https://doi.org/10.1017/hpl.2025.10084 Published online by Cambridge University Press

poised to unlock new frontiers in ultrafast science across disciplines.

References

1. Toshinori Suzuki. Time-resolved photoelectron spectroscopy of non-adiabatic electronic dynamics in gas and liquid phases. *International Reviews in Physical Chemistry*, 31(2):265–318, 2012.
2. Qin-Jun Peng, Nan Zong, Shen-Jin Zhang, Zhi-Min Wang, Feng Yang, Feng-Feng Zhang, Zu-Yan Xu, and Xing-Jiang Zhou. Duv/vuv all-solid-state lasers: twenty years of progress and the future. *IEEE Journal of Selected Topics in Quantum Electronics*, 24(5):1–12, 2018.
3. Zijian Cui, Mingying Sun, De'an Liu, and Jianqiang Zhu. High-peak-power picosecond deep-uv laser sources. *Opt. Express*, 30(24):43354–43370, Nov 2022.
4. Yukihiro Ozaki, Yusuke Morisawa, and Ichiro Tanabe. Atr-far-ultraviolet spectroscopy: a challenge to new σ chemistry. *Chemical Society Reviews*, 53(4):1730–1768, 2024.
5. Stefan Haacke and Irene Burghardt, editors. *Ultrafast Dynamics at the Nanoscale: Biomolecules and Supramolecular Assemblies*. Jenny Stanford Publishing, 2016.
6. Kong-Thon Tsen, editor. *Ultrafast Dynamical Processes in Semiconductors*, volume 92 of *Topics in Applied Physics*. Springer, 2004.
7. Shuai Fu, Heng Zhang, Klaas Jan Tielrooij, Mischa Bonn, and Hai I. Wang. Tracking and controlling ultrafast charge and energy flow in graphene–semiconductor heterostructures. *The Innovation*, 6(3):100764, 2025.
8. Stefan Roither, Xinhua Xie, Daniil Kartashov, Li Zhang, Markus Schöffler, Huailiang Xu, Atsushi Iwasaki, Tomoya Okino, Kaoru Yamanouchi, Andrius Baltuska, et al. High energy proton ejection from hydrocarbon molecules driven by highly efficient field ionization. *Physical review letters*, 106(16):163001, 2011.
9. Xinhua Xie, Stefan Roither, Markus Schöffler, Erik Lötstedt, Daniil Kartashov, Li Zhang, Gerhard G Paulus, Atsushi Iwasaki, Andrius Baltuška, Kaoru Yamanouchi, et al. Electronic predetermination of ethylene fragmentation dynamics. *Physical Review X*, 4(2):021005, 2014.
10. Xinhua Xie, Stefan Roither, Markus Schöffler, Huailiang Xu, Sergiy Bubin, Erik Lötstedt, Sonia Erattuphuza, Atsushi Iwasaki, Daniil Kartashov, Kálmán Varga, et al. Role of proton dynamics in efficient photoionization of hydrocarbon molecules. *Physical Review A*, 89(2):023429, 2014.
11. Sonia Erattupuzha, Seyedreza Larimian, Andrius Baltuška, Xinhua Xie, and Markus Kitzler. Two-pulse control over double ionization pathways in co2. *The Journal of Chemical Physics*, 144(2), 2016.
12. Seyedreza Larimian, Sonia Erattupuzha, Sebastian Mai, Philipp Marquetand, Leticia González, Andrius Baltuška, Markus Kitzler, and Xinhua Xie. Molecular oxygen observed by direct photoproduction from carbon dioxide. *Physical Review A*, 95(1):011404, 2017.
13. Xinhua Xie, Erik Lötstedt, Stefan Roither, Markus Schöffler, Daniil Kartashov, Katsumi Midorikawa, Andrius Baltuška, Kaoru Yamanouchi, and Markus Kitzler. Duration of an intense laser pulse can determine the breakage of multiple chemical bonds. *Scientific reports*, 5(1):12877, 2015.
14. Hongtao Hu, Yi Hung, Seyedreza Larimian, Sonia Erattupuzha, Andrius Baltuška, Markus Zeiler, and Xinhua Xie. Laser-induced valence electron excitation in acetylene. *Frontiers in Physics*, 10:1076671, 2022.
15. Sri Bhavya Muvva, Yusong Liu, Pratip Chakraborty, Joao Pedro Figueira Nunes, Andrew R. Attar, Surjendu Bhattacharyya, Kurtis Borne, Elio G Champenois, Nathan Goff, Kareem Hegazy, Matthias C Hoffmann, Fuhao Ji, Ming-Fu Lin, Duan Luo, Lingyu Ma, Asami Odate, Shashank Pathak, Daniel Rolles, Artem Rudenko, Sajib Kumar Saha, Xiaozhe Shen, Xijie Wang, Matthew R Ware, Stephen Weathersby, Peter M Weber, Kyle J Wilkin, Thomas J. A. Wolf, Yanwei Xiong, Xuan Xu, Jie Yang, Spiridoula Matsika, Thomas Weinacht, and Martin Centurion. Ultrafast structural dynamics of UV photoexcited cis , cis -1,3-cyclooctadiene observed with time-resolved electron diffraction. *Physical Chemistry Chemical Physics*, 27(1):471–480, dec 2024.
16. Jinquan Chen, Yuyuan Zhang, and Bern Kohler. Excited states in dna strands investigated by ultrafast laser spectroscopy. *Topics in Current Chemistry*, 356:39–88, oct 2015.
17. Pavel V. Kolesnichenko, Lukas Wittenbecher, Qiang Zhang, et al. Sub-100 fs formation of dark excitons in monolayer ws2. *Nano Letters*, 2024.
18. Sampriti Biswas, Ji Won Kim, Xiaoyuan Zhang, and Gregory D. Scholes. Coherent two-dimensional and broadband electronic spectroscopies. *Chemical Reviews*, 122(6):4727–4790, 2022.
19. Dimitar Popmintchev, Carlos Hernández-García, Franklin Dollar, Christopher Mancuso, Jose A. Pérez-Hernández, Ming-Chang Chen, Amelia Hankla, Xiaohui Gao, Bonggu Shim, Alexander L. Gaeta, Maryam Tarazkar, Dmitri A. Romanov, Robert J. Levis, Jim A. Gaffney, Mark Foord, Stephen B. Libby, Agnieszka Jaron-Becker, Andreas Becker, Luis Plaja,

https://doi.org/10.1017/hpl.2025.10084 Published online by Cambridge University Press

Margaret M. Murnane, Henry C. Kapteyn, and Tenio Popmintchev. Ultraviolet surprise: Efficient soft x-ray high-harmonic generation in multiply ionized plasmas. *Science*, 350(6265):1225–1231, 2015.
20. Yuika Saito. *Coupling of Deep-Ultraviolet Photons and Electrons*, pages 159–174. Springer Japan, Tokyo, 2015.
21. Deng haixiao, Wang xingtao, and Dai zhimin. Short-pulse length effects of the seed laser in high-gain harmonic generation free-electron laser. *Phys. Rev. ST Accel. Beams*, 11:040703, Apr 2008.
22. Paola Finetti, Hauke Höppner, Enrico Allaria, Carlo Callegari, Flavio Capotondi, Paolo Cinquegrana, Marcello Coreno, Riccardo Cucini, Miltcho B. Danailov, Alexander Demidovich, Giovanni De Ninno, Michele Di Fraia, Raimund Feifel, Eugenio Ferrari, Lars Fröhlich, David Gauthier, Torsten Golz, Cesare Grazioli, Yun Kai, Gabor Kurdi, Nicola Mahne, Michele Manfredda, Nikita Medvedev, Ivaylo P. Nikolov, Emanuele Pedersoli, Giuseppe Penco, Oksana Plekan, Mark J. Prandolini, Kevin C. Prince, Lorenzo Raimondi, Primoz Rebernik, Robert Riedel, Eleonore Roussel, Paolo Sigalotti, Richard Squibb, Nikola Stojanovic, Stefano Stranges, Cristian Svetina, Takanori Tanikawa, Ulrich Teubner, Victor Tkachenko, Sven Toleikis, Marco Zangrando, Beata Ziaja, Franz Tavella, and Luca Giannessi. Pulse duration of seeded free-electron lasers. *Phys. Rev. X*, 7:021043, Jun 2017.
23. E. Allaria, L. Badano, S. Bassanese, F. Capotondi, D. Castronovo, P. Cinquegrana, M. B. Danailov, G. D'Auria, A. Demidovich, R. De Monte, G. De Ninno, S. Di Mitri, B. Diviacco, W. M. Fawley, M. Ferianis, E. Ferrari, G. Gaio, D. Gauthier, L. Giannessi, F. Iazzourene, G. Kurdi, N. Mahne, I. Nikolov, F. Parmigiani, G. Penco, L. Raimondi, P. Rebernik, F. Rossi, E. Roussel, C. Scafuri, C. Serpico, P. Sigalotti, C. Spezzani, M. Svandrlik, C. Svetina, M. Trovó, M. Veronese, D. Zangrando, and M. Zangrando. The FERMI free-electron lasers. *Journal of Synchrotron Radiation*, 22(3):485–491, May 2015.
24. W Ackermann, G Asova, V Ayvazyan, A Azima, and Et al. Operation of a Free-Electron Laser from the Extreme Ultraviolet to the Water Window. *Nature Photonics*, 1:336–342, 2007.
25. P. Cinquegrana, A. Demidovich, G. Kurdi, I. Nikolov, P. Sigalotti, P. Susnjar, and M. B. Danailov. The seed laser system of the fermi free-electron laser: design, performance and near future upgrades. *High Power Laser Science and Engineering*, 9:e61, 2021.
26. Brian W.J. Mcneil and Neil R. Thompson. X-ray free-electron lasers. *Nature Photonics 2010 4:12*, 4(12):814–821, nov 2010.
27. A Dubietis, G. Tamošauskas, A. Varanavičius, G. Valiulis, and R. Danielius. Generation of femtosecond radiation at 211 nm by femtosecond pulse upconversion in the field of a picosecond pulse. *Optics Letters*, 25(15):1116, aug 2000.
28. Charles G. Durfee, Sterling Backus, Henry C. Kapteyn, and Margaret M. Murnane. Intense 8-fs pulse generation in the deep ultraviolet. *Optics Letters*, 24(10):697, may 1999.
29. Chun Zhou, Teruto Kanai, and Shuntaro Watanabe. Generation of ultrashort 90 μj deep-ultraviolet pulses by dual broadband frequency doubling with β-bab2o4 crystals at 1 khz. *Applied Physics Express*, 8(1):012701, dec 2014.
30. Chun Zhou, Teruto Kanai, Xiaoyang Wang, Yong Zhu, Chuangtian Chen, and Shuntaro Watanabe. Generation of ultrashort 25-μj pulses at 200 nm by dual broadband frequency doubling with a thin kbe2bo3f2 crystal. *Opt. Express*, 20(13):13684–13691, Jun 2012.
31. Waruna D Kulatilaka, James R Gord, and Sukesh Roy. Femtosecond two-photon lif imaging of atomic species using a frequency-quadrupled ti: sapphire laser. *Applied Physics B*, 116:7–13, 2014.
32. Peter Susnjar, Alexander Demidovich, Gabor Kurdi, Paolo Cinquegrana, Ivaylo Nikolov, Paolo Sigalotti, and Miltcho B. Danailov. A novel common-path scheme for fourth harmonic generation by ultrashort laser pulses. *Optics Communications*, 528:129031, 2023.
33. Michael Bauer. Femtosecond ultraviolet photoelectron spectroscopy of ultra-fast surface processes. *Journal of Physics D: Applied Physics*, 38(16):R253–R267, aug 2005.
34. U. Graf, M. Fieß, M Schultze, R. Kienberger, F. Krausz, and E. Goulielmakis. Intense few-cycle light pulses in the deep ultraviolet. *Optics Express*, 16(23):18956, nov 2008.
35. Takuya Horio, Roman Spesyvtsev, and Toshinori Suzuki. Simultaneous generation of sub-20 fs deep and vacuum ultraviolet pulses in a single filamentation cell and application to time-resolved photoelectron imaging. *Optics Express*, 21(19):22423, sep 2013.
36. Felix Köttig, Francesco Tani, Christian Martens Biersach, John C. Travers, and Philip St.J. Russell. Generation of microjoule pulses in the deep ultraviolet at megahertz repetition rates. *Optica*, 4(10):1272, oct 2017.
37. S V Makarov, A. N. Tsypkin, T. A. Voytova, V. A. Milichko, I. S. Mukhin, A. V. Yulin, S. E. Putilin, M. A. Baranov, A. E. Krasnok, I. A. Morozov, and P. A. Belov. Self-adjusted all-dielectric metasurfaces for deep ultraviolet femtosecond pulse generation. *Nanoscale*, 8(41):17809–17814, 2016.
38. Hongwen Xuan, Hironori Igarashi, Shinji Ito, Chen Qu, Zhigang Zhao, and Yohei Kobayashi. High-power, solid-state, deep ultraviolet laser generation. *Applied sciences*, 8(2):233, 2018.

https://doi.org/10.1017/hpl.2025.10084 Published online by Cambridge University Press

39. Gintaras Tamošauskas, Gvidas Beresnevičius, Darius Gadonas, and Audrius Dubietis. Transmittance and phase matching of bbo crystal in the 3−5 μm range and its application for the characterization of mid-infrared laser pulses. *Opt. Mater. Express*, 8(6):1410–1418, Jun 2018.
40. A M T Kim, C B Schaffer, C A D Roeser, and E Mazur. Two-Photon-Absorption FROG: Measuring White-Light Continuum Pulses. In *IEEE Conference on Lasers and Electro-Optics*. IEEE, 2001.
41. K. Ogawa and M. D. Pelusi. Characterisation of ultrashort optical pulses in a dispersion-managed fibre link using two-photon absorption frequency-resolved optical gating. *Optics Communications*, 198(1-3):83–87, oct 2001.
42. Kensuke Ogawa. Real-time intuitive spectrogram measurement of ultrashort optical pulses using two-photon absorption in a semiconductor. *Optics Express*, 10(5):262, mar 2002.
43. K. Ogawa, D. Kunimatsu, A. Suzuki, S. Arahira, Y. Kato, and Y. Ogawa. Pulse characterisation of a quantum-well mode-locked laser diode by two-photon absorption frequency-resolved optical gating. *Optical and Quantum Electronics*, 33(7-10):727–733, jul 2001.
44. R Trebino and D J Kane. Using phase retrieval to measure the intensity and phase of ultrashort pulses. *J. Opt. Soc. Am. A*, 10(5):1101–1111, 1993.
45. R Trebino. *Frequency-Resolved Optical Gating: The Measurement of Ultrashort Laser Pulses*. Springer, 2000.
46. Daniel J. Kane and Rick Trebino. Characterization of Arbitrary Femtosecond Pulses Using Frequency-Resolved Optical Gating. *IEEE Journal of Quantum Electronics*, 29(2):571–579, 1993.
47. N.G. Ivanov, V.F. Losev, M.V. Ivanov, and S.V. Alekseev. Femtosecond pulse width reduction upon second harmonic generation. *High Energy Density Physics*, 33:100701, 2019.
48. O. Gobert, G. Mennerat, R. Maksimenka, N. Fedorov, M. Perdrix, D. Guillaumet, C. Ramond, J. Habib, C. Prigent, D. Vernhet, T. Oksenhendler, and M. Comte. Efficient broadband 400nm noncollinear second-harmonic generation of chirped femtosecond laser pulses in bbo and lbo. *Appl. Opt.*, 53(12):2646–2655, Apr 2014.
49. Karoly Osvay and Ian N. Ross. Broadband sum-frequency generation by chirp-assisted group-velocity matching. *J. Opt. Soc. Am. B*, 13(7):1431–1438, Jul 1996.
50. Ida Z. Kozma, Peter Baum, Stefan Lochbrunner, and Eberhard Riedle. Widely tunable sub-30 fs ultraviolet pulses by chirped sum frequency mixing. *Opt. Express*, 11(23):3110–3115, Nov 2003.
51. M. A. Arbore, O. Marco, and M. M. Fejer. Pulse compression during second-harmonic generation in aperiodic quasi-phase-matching gratings. *Opt. Lett.*, 22(12):865–867, Jun 1997.
52. Makoto Aoyama, Tiejun Zhang, Motowo Tsukakoshi, and Koichi Yamakawa. Noncollinear second-harmonic generation with compensation of phase mismatch by controlling frequency chirp and tilted pulse fronts of femtosecond laser pulses. *Japanese Journal of Applied Physics*, 39(6R):3394, jun 2000.
53. R. H. French, J. W. Ling, F. S. Ohuchi, and C. T. Chen. Electronic structure of β-$\mathrm{bab_2o_4}$ and $\mathrm{lib_3o_5}$ nonlinear optical crystals. *Phys. Rev. B*, 44:8496–8502, Oct 1991.
54. Chuangtian Chen, Guiling Wang, Xiaoyang Wang, Yong Zhu, Zuyan Xu, Teruto Kanai, and Shuntaro Watanabe. Improved sellmeier equations and phase-matching characteristics in deep-ultraviolet region of $\mathrm{kbe_2bo_3f_2}$ crystal. *IEEE Journal of Quantum Electronics*, 44(7):617–621, 2008.
55. Xinhua Xie, Yunpei Deng, and Steven L Johnson. Compact and robust supercontinuum generation and post-compression using multiple thin plates. *High Power Laser Science and Engineering*, 9:e66, 2021.
56. Xinhua Xie, Adrian L Cavalieri, and Steven L Johnson. Self-compression of femtosecond laser pulses in ambient air through conical radiation. *Optics Letters*, 48(19):5101–5104, 2023.
57. Xinhua Xie, Yi Hung, Yunpei Deng, Adrian L Cavalieri, Andrius Baltuška, and Steven L Johnson. Generation of millijoule-level sub-5 fs violet laser pulses. *High Power Laser Science and Engineering*, 12:e16, 2024.

https://doi.org/10.1017/hpl.2025.10084 Published online by Cambridge University Press